2022

Experimental Studies on a Bubble Absorber with Swirl Entry of Refrigerant Vapour

Mani A Narasimha Reddy Sanikommu

Shaligram Tiwari

Experimental studies on a bubble absorber with swirl entry of refrigerant vapour

Narasimha Reddy Sanikommu, Mani A*, Shaligram Tiwari

Refrigeration and Air Conditioning Laboratory, Department of Mechanical Engineering, Indian Institute of Technology Madras, Tamil Nadu, India.

* Corresponding Author: Tel.:+91 44 22574666; fax: +91 44 22570509
Email address: mania@iitm.ac.in

ABSTRACT

Good heat and mass transfer rates in components like the absorber and generator are required to improve the overall performance of a vapour absorption refrigeration system (VARS). The present study carries out experimental investigations on an absorber to improve the heat and mass transfer characteristics during the absorption process. The heat and mass transfer characteristics of R134a (1, 1, 1, 2-tetrafluoroethane) vapour in DMF (dimethylformamide) liquid are studied using a copper tubular bubble absorber with swirl entry of refrigerant vapour. In order to create a swirling flow in an absorber, a cavity-type swirl generator is used in the present study. Hot water, cooling water and cooling load simulators are used to exchange the heat between VARS and the water medium. Experiments are carried out by altering the operating parameters, such as hot water temperature from 75^{o}C to 91^{o}C, cooling water temperature from 17^{o}C to 27^{o}C, weak solution flow rate from 0.04 m^3h^{-1} to 0.056 m^3h^{-1}, and liquid refrigerant flow rate from 0.005 m^3h^{-1} to 0.011 m^3h^{-1}. To understand the effects of weak solution flow rate and refrigerant flow rate on absorber performance, absorption rate, solution concentration at the outlet of the absorber, volumetric mass transfer coefficient, overall heat transfer coefficient, and absorber heat load have been evaluated.

1. INTRODUCTION

Vapour absorption refrigeration system (VARS) is an alternative refrigeration method that works based on low-grade energies like solar, geothermal, etc. VARS consists of four major heat and mass transfer components: evaporator, absorber, generator, and condenser. Because of the lower solution heat and mass transfer coefficients (Xie *et al.*, 2008) and substantial exergy destruction during the absorption process (Kilic and Kaynakli, 2007), the absorber is considered to be one of the critical components. The poor performance characteristics of the absorber result in poor performance of the VARS system. As a result, numerous enhancement techniques, including active and passive methods, have been used in the literature to improve the performance of an absorber. Experimental investigations have been conducted on a vertical tubular bubble absorber working with R22-DMF to explore the effect of operating parameters on the absorption phenomenon (Sujatha *et al.*, 1999). Suresh and Mani (2012) used a glass bubble absorber to study the heat and mass transfer characteristics of R134a in DMF. Effects of operating parameters, viz., gas flow rate, solution initial concentration, solution pressure, solution temperature and cooling water flow rate on absorber performance are investigated. Correlations for heat and mass transfer coefficients for R124-DMAC working pair in a copper vertical tubular bubble absorber have been developed by Jiang *et al.* (2017). Recently, an experimental study on heat and mass transfer characteristics of R124-NMO in a vertical glass bubble absorber has been conducted under operating conditions of an air-cooled absorption system (Wang *et al.*, 2020).

A single vertical nozzle (vapour distributor) is used in a tubular bubble absorber in all the studies reported above. In a double pipe heat exchanger, heat transfer is poor. This makes it challenging to use in absorption cooling systems (Cerezo *et al.*, 2018). Hence, simple passive and active enhancement techniques should help improve the heat and mass transfer rates, mainly in the absorber. Various studies that have been carried out in the literature to improve the absorption characteristics of the absorber in the VARS system are reported here. The absorption process in a bubble absorber has been enhanced by modifying absorber surface geometry, adding surfactants, nanoparticles and the

presence of external magnetic fields, etc. Experiments are being carried out to study the effect of advanced surfaces, i.e. internally micro-finned tube with internal helical micro-fins of 0.3 mm length with 20° helix angle on the ammonia absorption process in a tubular bubble absorber working with NH_3-$LiNO_3$. The absorption rate with a micro-finned tube is enhanced up to 1.7 times that with the smooth tube at a solution mass flow rate of 40 kgh^{-1} (Amaris *et al.*, 2014a). In addition, to improve the performance of an absorber, plate heat exchanger type bubble absorbers are used instead of a tubular bubble absorber (Oronel *et al.*, 2013, Suresh and Mani, 2013). An experimental comparison of the NH_3-H_2O bubble absorption process using a double tube heat exchanger with a helical screw static mixer in both the central and annular sides is conducted by Cerezo *et al.* (2018). According to the findings of the experiments, the absorber with a helical screw mixer absorbed 20% more vapour than the smooth tube. CFD studies are performed on an R134a-DMF tubular absorber with two tangential injectors having a 30° angle with a vertical axis to improve the efficiency of VARS (Panda and Mani, 2016). The heat and mass transfer coefficients are nearly 120%-170% and 20%-40% higher than that of the vertical nozzle in a bubble absorber.

Adding surfactants to working pairs causes surface gradients in solution and vapour, increasing heat and mass transfer rates due to the Marangoni effect (Kulankara and Herold, 2002). Similarly, adding nano-sized particles to base fluid improves the absorption rate due to increased thermal conductivity (Ma *et al.*, 2007). Effects of surfactants (n-octanol, 2-Octanol and 2E1H), surface roughness (micro-scale hatched tubes with a roughness of 0.39 µm and 6.97 µm) and binary nanoparticles (Cu, CuO and Al_2O_3) on absorption performance are studied on NH_3-H_2O system by Kim *et al.* (2006). The absorption rate for the bare tube with 700 ppm 2E1H surfactants is 4.8 times that of the bare tube without surfactants. The micro-scale hatched tube with surfactants has 4.5 times greater absorption performance than the bare tube without surfactants. The maximum effective absorption ratio of 3.21 is achieved with 0.01% Cu nanoparticles. Furthermore, both 2E1H and Cu nanoparticles improve the absorption rate by 5.32 times (Kim *et al.*, 2007). Experimental studies are carried out to estimate the individual and simultaneous effects of carbon nanotubes (CNT) and advanced surfaces on the performance of an NH_3-$LiNO_3$ tubular bubble absorber. The highest increase in absorption mass flux attained with CNT is around 1.64 times that obtained from plane tube. On the other hand, the simultaneous effect of CNT and advanced surfaces has increased the absorption mass flux by 1.8 times of that for the base fluid mixture and smooth tube (Amaris *et al.*, 2014b). Investigation of Fe_3O_4 nano ferrofluid in combination with the application of an external magnetic field on ammonia-water bubble absorber has revealed that the combined effect of the nano ferrofluid and the external magnetic field significantly enhanced ammonia-water bubble absorption greater than either technique alone under the same conditions. Under adiabatic conditions, the effective absorption ratio reached a maximum of 1.0812 ± 0.0001 with an initial ammonia mass concentration of 20%, a Fe_3O_4 nano ferrofluid mass concentration of 0.10% and external magnetic field intensity of 280 mT (Wu *et al.*, 2013). In the present study, heat and mass transfer studies on a bubble absorber working with R134a-DMF by employing a passive enhancement technique, namely a swirl generator (SG), are carried out to understand the absorption characteristics.

2. EXPERIMENTAL SETUP

The experimental setup is depicted schematically in Figure 1. The setup consists of VARS, a cooling load simulator, a cooling water simulator, a hot water tank simulator to mimic solar energy, and different measuring instruments, control devices and valves. The refrigerant vapour liberated from the generator storage tank (GT) is condensed in the condenser and stored in a liquid refrigerant storage tank. Condensation heat is removed using cooling water circulation. This liquid R134a from the liquid receiver is expanded through the throttle valve and evaporated in the evaporator by taking the heat from the chilled water supplied from the cooling load simulator. R134a vapour from the evaporator is absorbed in the absorber by the weak solution coming from the generator tank. The absorber is a tube in tube type exchanger with inner tube dimensions of 50 mm ID and 55 mm OD and outer tube dimensions of ID 65 mm and OD 75mm. R134a vapour is injected via a swirl generator installed at the bottom of the inner tube, and a weak solution from the generator storage tank is sent to the bottom of the inner tube. The heat of mixing during the absorption process is removed by cooling water from the cooling water simulator and supplied through the annulus of the absorber in the counter-flow direction. Due to the absorption of R134a vapour in a weak solution, the strong solution results at the absorber outlet and this strong solution is collected in the absorber storage tank. The strong solution from the absorber storage tank is pumped through a solution heat exchanger to the generator by a metering type solution pump. R134a vapour is boiled off in the generator due to the hot water supply, and it is separated in the generator storage tank. The weak solution in the generator storage tank is sent back to the absorber for absorption via a solution heat exchanger and pressure reducing valve. The solution heat exchanger is an add-on

component that transfers heat from a hot weak solution to a cool strong solution, hence reducing the amount of heat supplied to the generator.

Figure 2 illustrates the details of the swirl generator used in the present study (Sanikommu *et al.*, 2021). The swirl generator has four nozzles of the cavity profile shown in Figure 2a with a 0º camber angle and 20º twist angle. The authors have carried out bubble visualization studies to visualize the swirl motion created by SG. The cooling load simulator comprises a chilled water tank insulated with expanded polyethylene sheets (EPE), electric heaters, pump, flow meter, PT100 sensor, PID temperature controller, contactor, piping, and valves. The chilled water is used to supply the heat load in the evaporator, and the cooling load simulator is used to maintain a constant chilled water flow rate and temperature at the inlet of the evaporator. The cooling water simulator is made up of a cooling water tank with EPE insulation, vapour compression refrigeration system (VCRS), electric heaters, pump, flow meter, PT100 sensor, PID temperature controller, contactor, piping and valves. Cooling water simulator is used to supply cooling water in parallel to the absorber and condenser at a set temperature and flow rate. The hot water tank simulator consists of a hot water tank with glass wool insulation, electric heaters, pump, flow meter, PT100 sensor, PID temperature controller, contactor, piping and valves. This simulator sends hot water to the generator to liberate refrigerant vapour from a strong solution. Various measurement instruments, such as pressure transmitters, temperature sensors, flow meters, and online density meters, are installed at suitable locations, as shown in Figure 1. All of these measuring instruments have been pre-calibrated. Twenty-seven copper-constantan thermocouples are used as temperature sensors with ±1ºC uncertainty. Fourteen piezoelectric pressure transducers are used as pressure sensors with a measurement error of ±1.5%. The density of the strong and weak solutions is measured using an online density meter with a measurement uncertainty up to ±0.1 kgm^{-3}. Concentrations of weak and strong solutions are evaluated from the Hankinson-Brobst-Thomson (HBT) equation as reported by Reid *et al.* (1987) using the density values measured by an online density meter during the experiment. The readings are continuously monitored by integrating all of these instruments and sensors to a data acquisition system and a computer. Based on data measured during the experimental tests, performance evaluation of tubular absorber with swirl entry of refrigerant vapour has been performed.

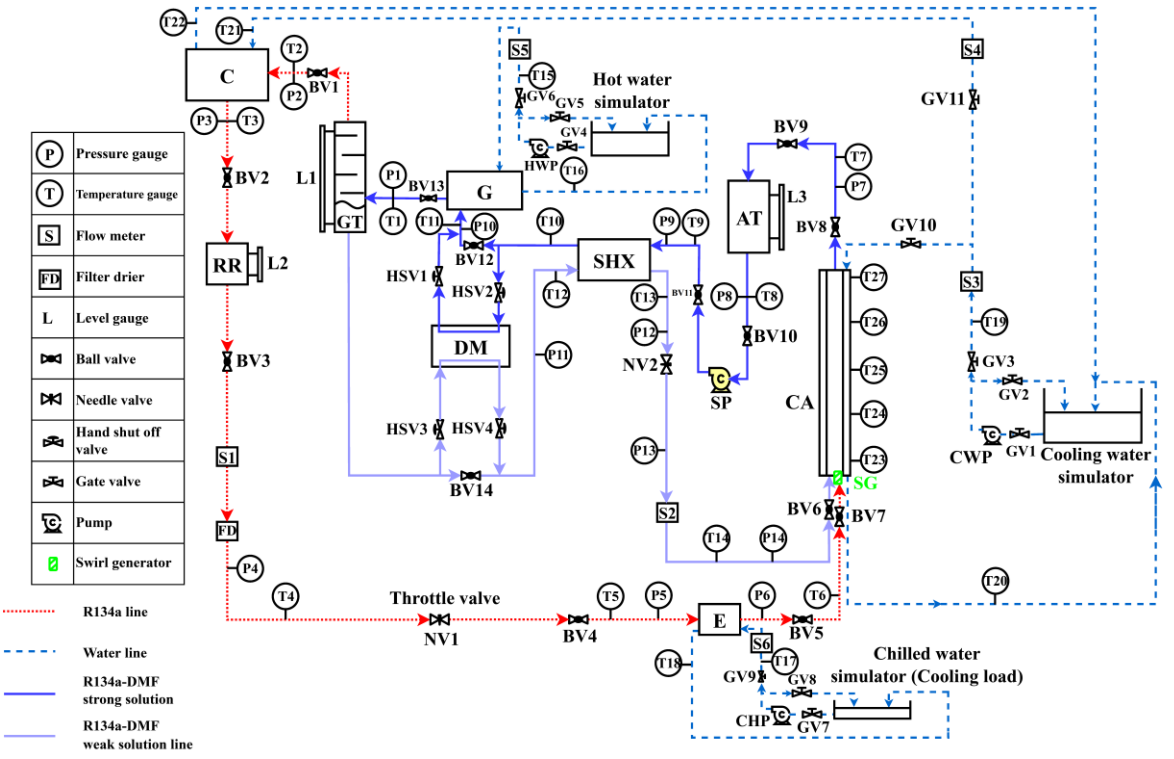

G - Generator; **GT**- Generator storage tank; **C**- Condenser; **RR**- Refrigerant reservoir; **E**- Evaporator; **CA**- Copper absorber; **AT**- Absorber tank; **DM**- Density meter

SHX- Solution heat exchanger; **SP**- Solution pump; **CWP**- Cooling water pump; **CHP**- Chilled water pump; **HWP**- Hot water pump; **SG** - Swirl generator

Figure 1: Schematic diagram of the experimental setup

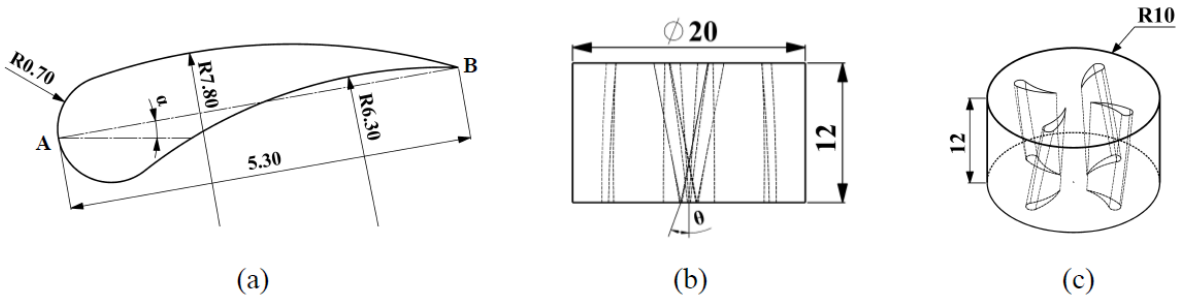

Figure 2: Details of the swirl generator (a) profile of the cavity (b) front view of SG (c) isometric view of SG (Sanikommu *et al*., 2021)

3. EXPERIMENTAL METHODOLOGY

The VARS system is initially charged with calculated R134a vapour and DMF liquid based on the system volume using the triple vacuum technique. The refrigerant and solution circuits are separated in the idle condition by closing the valves between the generator storage tank and condenser, evaporator and absorber. Simulators for hot and cooling water have been started. Hot water is supplied to the generator at a temperature higher than that to be maintained in the generator once the hot water has reached the prescribed temperature. Cooling water is circulated through the condenser and absorber in a parallel arrangement. Cooling water is sent at a temperature lower than the required temperature to be maintained in the respective components. A cooling load simulator is used to circulate the chilled water through an evaporator. Water temperature in the chilled water tank is maintained constant by operating the heaters same as the system's cooling capacity. Water flow rates in the hot water simulator, cooling water simulator, and cooling load simulator are kept constant. Then, the solution pump is switched on to supply the strong solution to a generator. The level of weak solution in the generator storage tank, the level of strong solution in the absorber tank and the pressure in each component of the solution circuit are continuously monitored. When the pressure in the generator storage tank surpasses the pressure in the condenser, the valve between them is opened to allow the refrigerant vapour to enter the condenser for condensation. The liquid R134a level in the liquid receiver is being checked. After collecting a sufficient amount of refrigerant liquid, it is allowed to enter the evaporator through the throttle valve. The valve between the evaporator and absorber is opened to allow refrigerant vapour to enter the absorber. Flow rates of weak solution and refrigerant are regulated to maintain a steady flow in the system. While the system is running, the readings of all the devices are continuously monitored, and steady-state readings are recorded on the computer when all of these readings remain constant over time. Experimental tests are repeated for different operating conditions, i.e. different hot water temperatures, cooling water temperatures, weak solution flow rates and refrigerant liquid flow rates. Finally, the solution and refrigeration circuits are isolated by closing appropriate valves while shutting down the system after the experimental tests are completed. Then the solution pump is switched off, as well as all of the simulators.

4. RESULTS AND DISCUSSION

Experiments with a cooling capacity of 3.4 kW are carried out by varying the operating parameters, such as weak solution flow rate from 0.04 m^3h^{-1} to 0.056 m^3h^{-1}, liquid refrigerant flow rate from 0.005 m^3h^{-1} to 0.011 m^3h^{-1}, hot water temperature from 75°C to 91°C, cooling water temperature from 17°C to 27°C. Water flow rates are maintained constant at 0.1 m^3h^{-1} for hot water, 0.08 m^3h^{-1} for absorber cooling water, 0.0775 m^3h^{-1} for condenser cooling water and 0.0475 m^3h^{-1} for chilled water. The performance parameters, including absorber heat transfer rate, overall heat transfer coefficient, absorption rate, and volumetric mass transfer coefficient, have been studied by varying solution and refrigerant flow rates by keeping all other parameters constant. These quantities are defined in Appendix. All of the results presented here are for a hot water temperature of 90.6°C, cooling water at 17°C temperature and chilled water temperature of 31.1°C.

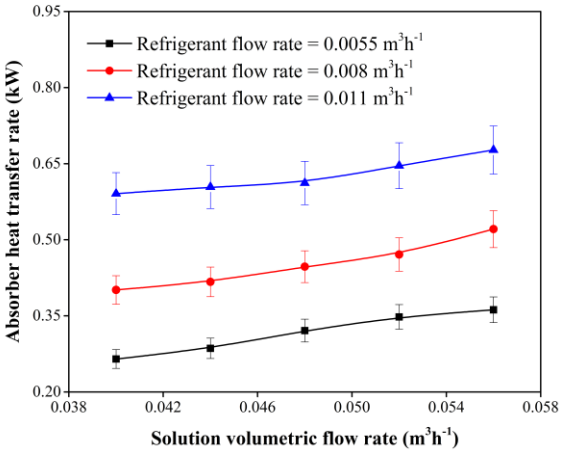

Figure 3: Effect of refrigerant and weak solution flow rates on absorber heat transfer rate

Figure 3 illustrates the heat transfer rate in the absorber as a function of weak solution flow rate for various refrigerant flow rates. The absorber heat transfer rate increases as refrigerant flow increases because of high absorption rates and increased heat of mixing during the absorption process. The heat transfer rate in the absorber increases with an increase in weak solution flow rate due to increased weak solution mass flow rate and an increased overall heat transfer coefficient which is evident from Figure 4. An increase in refrigerant flow rate causes more vapour bubbles in the solution, resulting in increased heat transfer and a higher overall heat transfer coefficient. Similarly, as the weak solution flow rate increases, convective heat transfer in the absorber increases, which results in an increased overall heat transfer coefficient with the solution flow rate. As a result, with weak solution and refrigerant flow rates, the overall heat transfer coefficient of the absorber increases. Figure 5 depicts the variation of solution pressure drop with weak solution flow rate for different refrigerant flow rates. It is seen that with the weak solution and refrigerant flow rates, the solution pressure drop increases. This is due to an increase in flow velocity and friction due to the increase in weak solution and refrigerant flow rates.

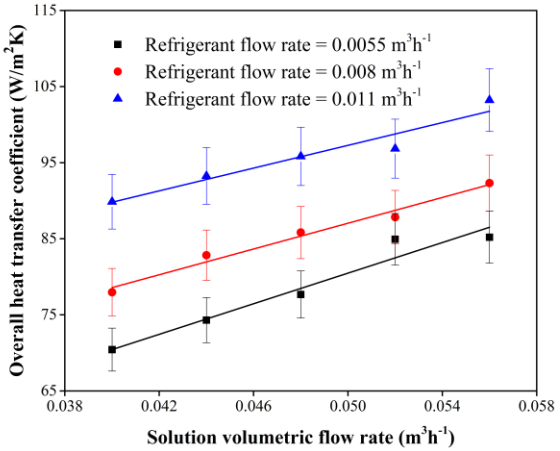

Figure 4: Variation of overall heat transfer coefficient with weak solution and refrigerant flow rates

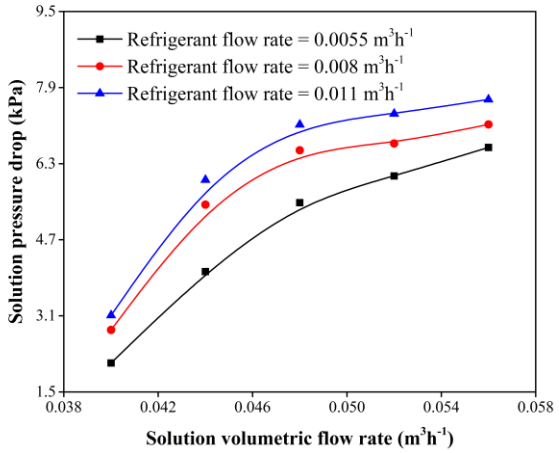

Figure 5: Effect of weak solution flow rate on solution pressure drop for different refrigerant flow rates

Figure 6 shows the effect of refrigerant flow rate on solution concentration at the absorber outlet for various weak solution flow rates. As the gas flow rate increases, the amount of absorbed refrigerant vapour increases for a given amount of weak solution, resulting in increased solution concentration at the outlet of the absorber. However, at higher weak solution flow rates, the concentration decreases due to the dilution of the solution with a weak solution. As a result, the concentration difference between strong and weak solutions increases as the refrigerant flow rate increases. In addition, the concentration difference reduces as the solution flow rate increases, as seen in Figure 7.

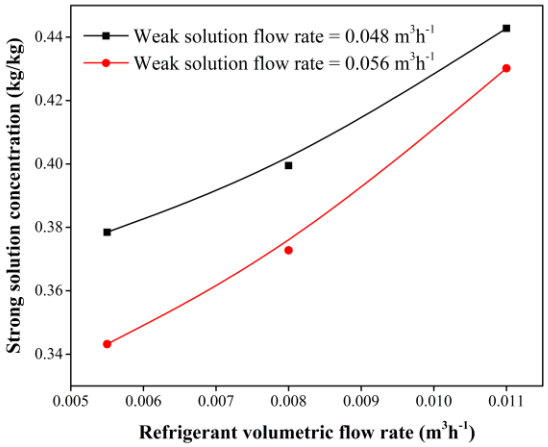

Figure 6: Effect of refrigerant flow rate on absorber outlet concentration for various weak solution flow rates

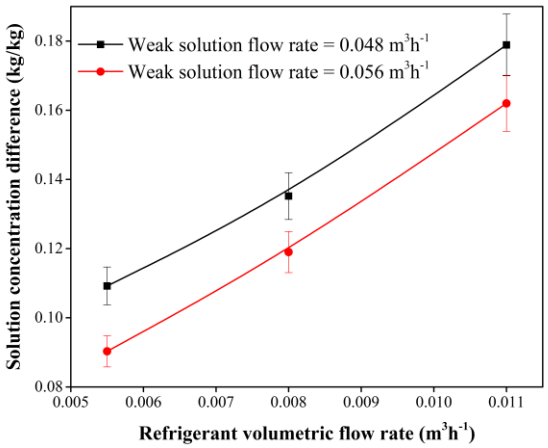

Figure 7: Variation of solution concentration difference with weak solution and refrigerant flow rates

The absorption rate varies with refrigerant and weak solution flow rates, as shown in Figure 8. The amount of refrigerant vapour absorbed in the weak solution increases as refrigerant flow increases, resulting in high absorption rates. Furthermore, with high weak solution flow rates, the quantity of solution available for gas absorption is more, resulting in a higher absorption rate. As the refrigerant flow rate increases, the initial turbulence, mixing, and the mean interfacial velocity also increase, causing the mass transfer rate to increase, leading to an increased volumetric mass transfer coefficient, as shown in Figure 9. The increase in the weak solution flow rate means the decrease in the average mass fraction of the solution in the absorber, which causes the average mass transfer driving potential to increase. As a result, the volumetric mass transfer coefficient increases with an increase in the weak solution flow rate.

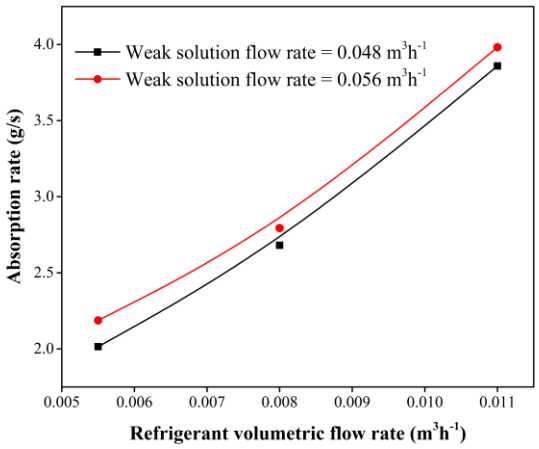

Figure 8: Effect of refrigerant and weak solution flow rates on the absorption rate

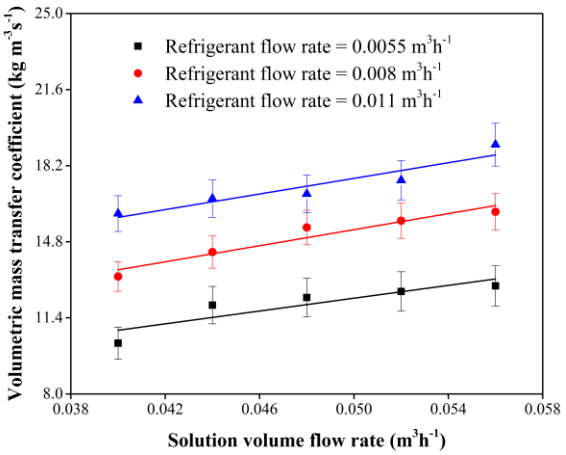

Figure 9: Effect of weak solution flow rate on volumetric mass transfer coefficient for different refrigerant flow rates

6. CONCLUSIONS

The present work reports experimental studies on heat and mass transfer characteristics of a tubular copper absorber with swirl entry of refrigerant vapour. The cavity type swirl generator is used in this study, and it has a 0° camber angle and 20° twist angle. By varying solution and refrigerant flow rates while maintaining all other parameters constant, performance parameters like volumetric mass transfer coefficient, overall heat transfer coefficient, absorber heat load, concentration difference and pressure drop are examined. The absorption heat transfer rate, absorption rate, overall heat transfer coefficient, volumetric mass transfer coefficient and solution pressure drop increased with an increase in refrigerant and weak solution flow rates. Solution concentration at the absorber outlet and concentration difference across the absorber are found to increase as the refrigerant flow rate increases and the weak solution flow rate decreases.

NOMENCLATURE

Cp	specific at constant pressure	$(kJkg^{-1}K^{-1})$
D	absorber inner tube diameter	(m)
h	enthalpy	$(kJkg^{-1})$
ID	inner diameter	(m)
$k_l a$	volumetric mass transfer coefficient	$(kgm^{-3}s^{-1})$
L	length of absorber	(m)
LMCD	logarithmic concentration difference	(-)
LMTD	logarithmic mean temperature difference	(-)
m	mass flow rate	(kgs^{-1})
OD	outer diameter	(m)
Q	heat transfer rate	(W)
R	radius	(m)
T	temperature	(°C)
U	overall heat transfer coefficient	$(Wm^{-2}K^{-1})$
V	volume flow rate	(m^3h^{-1})
X	liquid mass fraction	$(kgkg^{-1})$
α	camber angle	(°)
θ	twist angle	(°)

Subscript

A, a	absorption

ai	equivalent absorber inlet temperature
cw	cooling water
eq	equilibrium
l	liquid
r	refrigerant
ss	strong solution
ws	weak solution
1	inner
2	outer

APPENDIX A

Heat rejected in the absorber to cooling water: $Q_a = m_{cw} C_{p,cw} (T_{20} - T_{19})$ (1)

Logarithmic mean temperature difference: $LMTD = \frac{(T_{ai} - T_{20}) - (T_7 - T_{19})}{\ln\left(\frac{T_{ai} - T_{20}}{T_7 - T_{19}}\right)}$ (2)

where T_{ai} is the equivalent solution temperature at the inlet of the absorber corresponding to $h_{ai} = \frac{m_r h_6 + m_{ws} h_{14}}{m_r + m_{ws}}$

Overall heat transfer coefficient: $U_o = \frac{Q_a}{(\pi D_2 L) LMTD}$ (3)

Absorption rate: $m_a = \frac{m_{ws}(X_{ss} - X_{ws})}{X_r - X_{ss}}$ (4)

Logarithmic mean concentration difference: $LMCD = \frac{(X_{eq,ss} - X_{ss}) - (X_{eq,ws} - X_{ws})}{ln\left(\frac{X_{eq,ss} - X_{ss}}{X_{eq,ws} - X_{ws}}\right)}$ (5)

Volumetric mass transfer coefficient: $k_l a = \frac{m_a}{\left(\frac{\pi}{4} D_1^2 L\right) LMCD}$ (6)

APPENDIX B

Uncertainity in derived quatities

Heat transfer rate: $\frac{\delta Q_a}{Q_a} = \left[\left(\frac{\delta V_{cw}}{V_{cw}}\right)^2 + 2\left(\frac{\delta T}{T}\right)^2\right]^{1/2} = [(0.05)^2 + 2(0.0416)^2]^{1/2} = \pm 7.72\%$

Overall heat transfer coefficient: $\frac{\delta U_o}{U_o} = \left[\left(\frac{\delta Q_a}{Q_a}\right)^2 + 2\left(\frac{\delta T}{T}\right)^2\right]^{1/2} = [(0.0772)^2 + 2(0.0416)^2]^{1/2} = \pm 9.70\%$

Absorption rate: $\frac{\delta m_a}{m_a} = \left[\left(\frac{\delta V_{ws}}{V_{ws}}\right)^2 + \left(\frac{\delta V_r}{V_r}\right)^2\right]^{1/2} = [(0.05)^2 + (0.0595)^2]^{1/2} = \pm 7.77\%$

Volumetric mass transfer coefficient: $\frac{\delta k_l a}{k_l a} = \left[\left(\frac{\delta m_a}{m_a}\right)^2 + 2\left(\frac{\delta X}{X}\right)^2\right]^{1/2} = [(0.0707)^2 + 2(0.0267)^2]^{1/2} = \pm 8.01\%$

REFERENCES

Amaris, C., Bourouis, M., & Vallès, M. (2014a). Effect of advanced surfaces on the ammonia absorption process with NH3/LiNO3in a tubular bubble absorber. *International Journal of Heat and Mass Transfer*, *72*, 544–552.

Amaris, C., Bourouis, M., & Vallès, M. (2014b). Passive intensification of the ammonia absorption process with NH3/LiNO3using carbon nanotubes and advanced surfaces in a tubular bubble absorber. *Energy*, *68*, 519–528.

Cerezo, J., Best, R., Chan, J. J., Romero, R. J., Hernandez, J. I., & Lara, F. (2018). A theoretical-experimental comparison of an improved ammonia-water bubble absorber by means of a helical static mixer. *Energies*, *11*(1), 1–14.

Jiang, M., Xu, S., & Wu, X. (2017). Experimental investigation for heat and mass transfer characteristics of R124-DMAC bubble absorption in a vertical tubular absorber. *International Journal of Heat and Mass Transfer*, *108*, 2198–2210.

Kilic, M., & Kaynakli, O. (2007). Second law-based thermodynamic analysis of water-lithium bromide absorption refrigeration system. *Energy*, *32*(8), 1505–1512.

Kim, J. K., Jung, J. Y., & Kang, Y. T. (2007). Absorption performance enhancement by nanoparticles and chemical surfactants in binary nanofluids. *International Journal of Refrigeration*, *30*(1), 50–57.

Kim, J. K., Jung, J. Y., Kim, J. H., Kim, M. G., Kashiwagi, T., & Kang, Y. T. (2006). The effect of chemical surfactants on the absorption performance during NH3/H2O bubble absorption process. *International Journal of Refrigeration*, *29*(2), 170–177.

Kulankara, S., & Herold, K. E. (2002). Surface tension of aqueous lithium bromide with heat/mass transfer enhancement additives : the effect of additive vapor transport. *International Journal of Refrigeration*, *25*, 383–389.

Oronel, C., Amaris, C., Bourouis, M., & Vallès, M. (2013). Heat and mass transfer in a bubble plate absorber with NH3/LiNO3and NH3/(LiNO3+ H2O) mixtures. *International Journal of Thermal Sciences*, *63*, 105–114.

Panda, S. K., & Mani, A. (2016). CFD Heat and Mass Transfer Studies in a R134a- DMF Bubble Absorber with Swirl Flow Entry of R134a Vapour. *16th International Refrigeration and Air Conditioning Conference at Purdue, July 11-14, 2043*, 1–10.

Reid, R. C., Prausnitz, J. M., & P. B. E. (1987). *The properties of gases and liquids* (Fourth). McGraw-Hill, New York.

Sanikommu, N. R., Mani, A., & Tiwari, S. (2021). Bubble dynamics studies in an absorber with swirl entry of an absorption refrigeration system. *18th International Refrigeration and Air Conditioning Conference at Purdue, May 24-28, 2393*, 1–9.

Sujatha, K. S., Mani, A., & Murthy, S. S. (1999). Experiments on a bubble absorber. *International Communications in Heat and Mass Transfer*, *26*(7), 975–984.

Suresh, M., & Mani, A. (2012). Experimental studies on heat and mass transfer characteristics for R134a-DMF bubble absorber. *International Journal of Refrigeration*, *35*(4), 1104–1114.

Suresh, M., & Mani, A. (2013). Heat and mass transfer studies on a compact bubble absorber in R134a-DMF solution based vapour absorption refrigeration system. *International Journal of Refrigeration*, *36*(3), 1004–

Wang, W., Xu, S., Wu, X., & Jiang, M. (2020). Experimental investigation on heat and mass transfer in a vertical glass bubble absorber with R124-NMP pair. *International Journal of Refrigeration*, *112*, 303–313.

Wu, W. D., Liu, G., Chen, S. X., & Zhang, H. (2013). Nanoferrofluid addition enhances ammonia/water bubble absorption in an external magnetic field. *Energy and Buildings*, *57*, 268–277.

Xie, G., Sheng, G., Bansal, P. K., & Li, G. (2008). Absorber performance of a water/lithium-bromide absorption chiller. *Applied Thermal Engineering*, *28*(13), 1557–1562.

Xuehu, M., Su, F., Chen, J., & Zhang, Y. (2007). Heat and mass transfer enhancement of the bubble absorption for a binary nanofluid. *Journal of Mechanical Science and Technology*, *21*(11), 1813–1818.